THE JOURNAL OF PHYSICAL CHEMISTRY B

Article

pubs.acs.org/JPCB

Orientation of Carbon Fiber Axes in Polymer Solutions under Magnetic Field Evaluated in Terms of Orientation Distribution of the Chain Axes of Graphite with Respect to the Carbon Fiber Axis

Masaru Matsuo,*[,†] Yumiko Takemoto (Nakano),[‡] Rong Zhang,[†] Jun Liu,[†] Ru Chen,[†] and Yuezhen Bin[†]

[†]Department of Polymer Material Science, Dalian University of Technology, Dalian 116024, People's Republic of China

[‡]Department of Human Environmental Sciences, School of Human Environmental Sciences, Mukogawa Women's University, Ikebiraki-cho, Nishinomiya 663-8558, Japan

ABSTRACT: Orientation of carbon fiber (CF) axes in poly(vinyl alcohol) (PVA) aqueous solution under magnetic field was evaluated by considering the fact that the *c*-axes (chain axes of graphite) have orientation distribution with respect to their CF axis. This new approach was proposed to resolve the well-known contradiction that the diffraction image from the (002) plane measured by X-ray shows broad arcs indicating dull orientation of the *c*-axes with respect to the magnetic field, whereas the corresponding orientation of CF axes observed by SEM reveals high predominant orientation. To pursue the quantitative evaluation, the orientation function of CF axes was obtained from the orientation function of the reciprocal lattice vector of the (002) plane by a somewhat coordinate transformation. The real orientation function of the CF axes with respect to the magnetic field direction showed very sharp distribution profile in comparison to the function of the *c*-axes and it was in good agreement with the orientation of CF axes observed directly by SEM. Furthermore, the orientation of CF axes up to the equilibrium state was estimated by a common diffusion equation. The calculated results predicted time dependence of the preferential orientation behavior of CFs in PVA solution precisely.

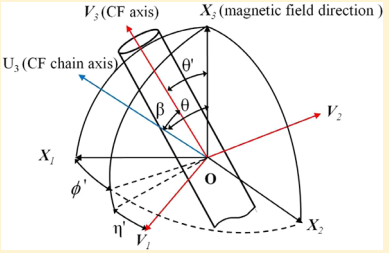

1. INTRODUCTION

In previous paper,[1] the orientation behavior of carbon fibers (CFs) in polymer solution/gel under magnetic field was proposed in terms of orientation distribution function of the measurable reciprocal lattice vector of the (002) plane (the [002] direction) by using the composite films, because the estimations for a number of papers concerning orientation of CFs[2,3] and carbon nanotubes[4−9] had been done in terms of the second-order orientation factor of the [002] direction and/or direct observation by scanning electron microscopy (SEM). The previous paper was the first successful work for the direct estimation of orientation of CF axes within the dried film in terms of orientation function by considering an uniaxial (random) orientation of the CF axes around the magnetic field direction as well as a random rotation of CF around its own axis.[1] The composites were prepared by gelation/crystallization from dispersed poly(vinyl alcohol) (PVA)−CF solution and by evaporation of solvent from the gel under magnetic field.

According to established papers,[2,3] however, the wide-angle X-ray diffraction (WAXD) from the (002) plane reveals broad arcs, indicating gradual orientation function of the CF axes with respect to the magnetic field direction, when an X-ray beam was directed parallel to the film surface. On the other hand, the corresponding reported SEM images have shown high aligned CFs with respect to the magnetic field direction. The previous paper pointed out that such contradiction is attributed to the fact that the proposed evaluation method can be utilized only in a very special case where most of the *c*-axes (chain axes) of graphite are aligned perfectly along their CF axis, but the actual orientation of the *c*-axes have orientation distribution with respect to the CF axis. In preliminary experiments,[10] the Young's modulus of the long CF before the cutting was ca. 250 GPa lower than crystal lattice modulus (1050 GPa) and the WAXD pattern showed the broad diffraction arcs from graphite structure and/or turbostractic structure denoting imperfect graphites. Furthermore, the corresponding small-angle X-ray scattering lobes with the first-order scattering maximum were extended in the horizontal direction, indicating the preferential orientation of the long axis of ellipsoidal voids with respect to the CF (machine) direction.

By considering the orientation distribution of CF chain axes with respect to the CF axis, this paper is concerned with the theoretical calculation of the CF axes with respect to the magnetic field as one of general categories to resolve the discrepancy between WAXD and SEM images. The present system represents the orientation fluctuation of the chain axes with respect to the CF axis to throw up further precise development of the previous mathematical evaluation. Somewhat complicated mathematical evaluation is proposed to formulate the general polymer-nanocomposite systems (especially triclinic crystal unit) in Appendix. This paper, however, emphasizes that the complicated general formulation reduces to the simplest treatment on applying to CFs because of hexagonal crystal unit of graphite. The geometrical analysis provides sharp

Received: October 16, 2012
Revised: January 21, 2013
Published: January 23, 2013

dx.doi.org/10.1021/jp310239q | *J. Phys. Chem. B* 2013, 117, 2516−2526

orientation distribution of CF axes with respect to the magnetic field direction and the sharp orientation of the CF axes is found to be in good agreement with observed SEM images.

2. EXPERIMENTAL SECTION

The long CFs (used as specimen D in ref 10) were cut and the resultant short CFs, their average length and average diameter being 45 and 5.0 μm, respectively, were dispersed into PVA solution, as described in the previous paper.[1] Their average sizes were determined by SEM observation. The average volume of CF was estimated to be 8.8×10^2 μm^3.

The orientation function of the [002] direction with respect to the CF axis was measured by using the long CFs whose characterization was reported already,[10] but the more precise measurement was carried out again in the present paper to check the creditability to pursue more complicated mathematical analysis. The measurement was done by WAXD instrument with 12 kW rotating anode X-ray generator (Rigaku RAD-rA).

To make clear the essential difference in the previous and present investigations, the main experimental procedure was also summarized again briefly in the present paper. That is, PVA (polymerization of 2000 and 98% hydrolyzed) was used as matrix. PVA-CF composites were prepared by gelation/crystallization from solutions in a dimethyl sulfoxide (DMSO) and water mixture. The DMSO/water composition was set to be 60/40, assuring rapid gelation and stiff gel. The contents of CFs against the mixed solvent were 1.0% and 2.5%, in which the concentration of PVA against the mixed solvent was fixed to be 10 g/100 mL. Furthermore, 1.0% CF content was prepared for 13 g/100 mL solution. Three kinds of dispersion solutions were prepared by stirring at 105 °C, which were named as 1.0% CF in 10% PVA, 1.0% CF in 13% PVA, and 2.5% CF in 10% PVA. The each well-dispersed solution was poured into a Petri dish set under magnetic field with 0.46 T whose magnetic field direction was perpendicular to the dish. The gelation occurred within 2 h after cooling to room temperature (ca. 25 °C) and the resultant gels were kept to evaporate the mixed solvent for 3 days. After then, they were immersed in a water bath for 1 day to remove the trace of the mixed solvent and were dried at room temperature.

The orientation behavior of CFs within the resultant composite was estimated by X-ray diffraction technique. Of course, as discussed in the previous paper,[1] the orientation of CFs in the resultant composite is assumed to be equivalent to the orientation of CFs in the solution, independent of solvent evaporation under magnetic field.

3. RESULTS AND DISCUSSION

3.1. SEM and WAXD Images and Orientation Function in the [002] Direction. Figure 1 shows three WAXD images (end view) on the left side and the corresponding SEM images on the right side. In column a, the SEM image shows almost perfect orientation of CFs with respect to the magnetic field direction but the corresponding WAXD image reveals slightly broad arcs from the (002) plane indicating no perfect orientation of the *c*-axes of graphite crystallites. Generally, it is well-known that polyethylene fibrils in ultradrawn polyethylene film are oriented predominantly under SEM observation and the corresponding diffractions from the (110) and (200) planes reveal sharp spots in the horizontal direction.[11] Curiously, as shown in columns b and c, the CFs orient predominantly with respect to the magnetic field direction under SEM but the corresponding diffraction from the (002) plane reveal very broad

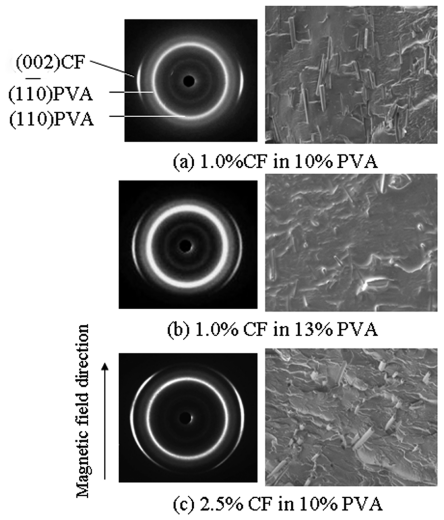

Figure 1. WAXD patterns (end view) and SEM images for the PVA-CF shown on the left and right sides, respectively, in which the films were prepared from (a) 1.0% CF in 10% PVA solution, (b) 1.0% CF in 13% PVA solution, and (c) 2.5% CF in 10% PVA solution.

arcs, indicating very broad orientation of the *c*-axes. In spite of the well-known contradiction,[2,3] such profiles have been reported without any comments by several authors. The reason is due to the laboriousness to pursue the precise mathematical evaluation. Accordingly, the evaluation has remained an unresolved problem. To solve this difficult problem, the detailed orientation of the *c*-axes with respect to the CF axis was estimated.

Figure 2 shows the orientation distribution function $2\pi q_j'(\cos\theta_{[002]}')$ of the reciprocal lattice vector of the (002)

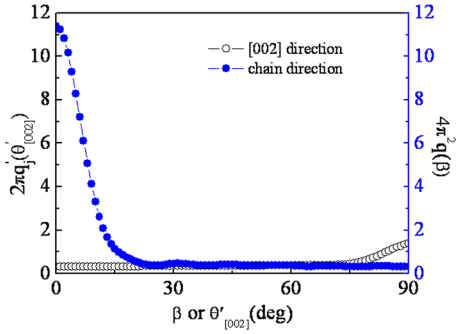

Figure 2. Orientation distribution function $2\pi q_j'(\cos\theta_{[002]}')$ of the reciprocal lattice vector of the (002) plane (the [002] direction) represented as open circles and orientation distribution function $4\pi^2 q(\cos\beta)$ (solid circles) of the *c*-axes calculated by eqs 6–9.

plane (the [002] direction) with respect to the CF axis as open circles and the orientation function $4\pi^2 q(\cos\beta)$ of the *c*-axes as solid circles.

First of all, as described elsewhere,[1,10] $2\pi q_j'(\cos\theta_{[002]}')$ can be obtained as follows:

$$q_j'(\theta_{[002]}') = \frac{I_{[002]}'(\theta_{[002]}')}{\int^{2\pi}\int_0^{\pi} I_{[002]}'(\theta_{[002]}')\sin\theta_{[002]}'\,d\theta_{[002]}'\,d\phi_{[002]}'} = \frac{I_{[002]}'(\theta_{[002]}')}{2\pi\int_0^{\pi} I_{[002]}'(\theta_{[002]}')\sin\theta_{[002]}'\,d\theta_{[002]}'} \quad (1)$$

dx.doi.org/10.1021/jp310239q | J. Phys. Chem. B 2013, 117, 2516–2526

where $I'_{[002]}(\theta'_{[002]})$ is X-ray diffraction intensity distribution as a function of $\theta'_{[002]}$ denoting polar angle between the reciprocal lattice vector and the CF axis.

Then the orientation factors can be given by

$$F_{l0}^{[002]'} = \int_0^{\pi} q'_j(\theta'_{[002]})\, P_l(\cos\theta'_{[002]})\, \sin\theta'_{[002]}\, \mathrm{d}\theta'_{[002]} \tag{2}$$

As for a graphite crystal unit, the [002] direction perpendicular to the *c*-axis takes uniaxial orientation around the magnetic field and random rotation around the *c*-axis. Hence the orientation function of the *c*-axes with respect to the CF axis can be calculated in accordance with the previous evaluation.[10] That is,

$$4\pi^2 q(\beta) = \frac{1}{2} + 2\sum_{l=2}^{\infty} G_{l00} P_l(\cos\beta) \tag{3}$$

where

$$G_{l00} = \frac{F_{l0}^{[002]'}}{P_l(1)} \tag{4}$$

where $P_l(x)$ is the Legendre polynomial.

The orientation function $4\pi^2 q(\cos\beta)$ of the *c*-axes reveals the predominant orientation distribution with respect to the CF axis. The estimation of $4\pi^2 q(\cos\beta)$ is very important to analyze the orientation of CF axes with respect to the magnetic field direction, because the previous estimation[1] was done by assuming perfect orientation of the chain axes with respect to the CF axis, that is, $q(\cos\beta) = 0$ at $\beta \neq 0°$. The difference between SEM and WAXD images as shown in Figure 1 is due to the fact that the orientation distribution of *c*-axes (crystal chain axes) with respect to the CF axis has been neglected because of the very complicated mathematical evaluation. Based on the concept, the precise mathematical treatment can be represented in relation to general evaluation in Appendix.

3.2. Theoretical Background. First of all, a general mathematical representation of orientation distribution functions of crystal unit cell and reciprocal lattice vector are given in terms of series expansions of the functions in generalized spherical harmonics,[12−16] because the present system for orientation CF axes with respect to the magnetic field can be contained in this proposed general category. Based on the concept, a complete mathematical description for the relationship between crystal unit and crystal block (as like reinforced fiber) may be treated by using Figure 3. Figure 3a shows the geometrical interrelation of a Cartesian coordinate O-$U_1U_2U_3$ of crystal unit cell fixed within a Cartesian coordinate O-$X_1X_2X_3$ of the bulk specimen. The orientation of crystal unit within the space of the film specimen may be specified by using three Euler angles, θ, ϕ, and η. The angles θ and ϕ, which define the orientation of U_3 axis of the unit within the space, are the polar and azimuthal angles, respectively, and η specifies the rotation of the unit around its own U_3 axis. Figure 3b shows the geometrical interrelation of a Cartesian coordinate O-$V_1V_2V_3$ of crystal block fixed within a Cartesian coordinate O-$X_1X_2X_3$ of the bulk specimen. Euler angles θ', ϕ', and η' correspond to Euler angles θ, ϕ, and η in Figure 3a. Figure 3c shows the geometrical interrelation of a Cartesian coordinate O-$U_1U_2U_3$ of crystal unit cell fixed within a Cartesian coordinate O-$V_1V_2V_3$ of crystal block, in which Euler angles β, α, and γ correspond to Euler angles θ, ϕ, and η in Figure 3a.

In accordance with a general mathematical procedure of the three Cartesian coordinates in Figure 3, the normalized

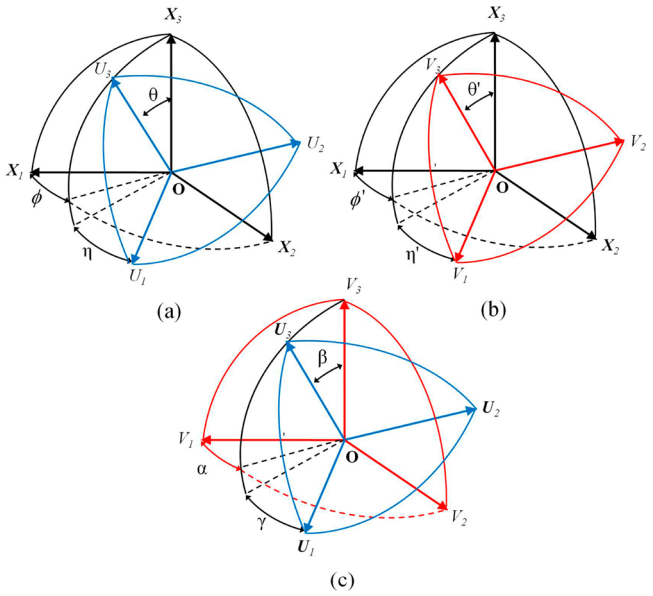

Figure 3. (a) Geometrical interrelation of a Cartesian coordinate O-$U_1U_2U_3$ of the crystal unit cell fixed within a Cartesian coordinate O-$X_1X_2X_3$ of bulk specimen, in which Euler angles θ and ϕ are the polar and azimuthal angles, respectively, and η specifies the rotation of the unit around its own U_3 axis. (b) Geometrical interrelation of a Cartesian coordinate O-$V_1V_2V_3$ of crystal block fixed within a Cartesian coordinate O-$X_1X_2X_3$ of bulk specimen. (c) Geometrical interrelation of a Cartesian coordinate O-$U_1U_2U_3$ of crystal unit cell fixed within a Cartesian coordinate O-$V_1V_2V_3$ of crystal block.

orientation distribution functions $\omega(\theta,\phi,\eta)$ of the crystal unit fixed within the film, $\omega'(\theta',\phi',\eta')$ of crystal block fixed within the specimen, and $q(\beta,\alpha,\gamma)$ of crystal unit fixed within the crystal block may be expressed in a series of generalized spherical harmonics as follows:

$$\omega(\theta,\phi,\eta) = \sum_{l=0}^{\infty}\sum_{m=-l}^{l}\sum_{n=-l}^{l} W^*_{lmn} Z_{lmn}(\cos\theta)\exp\{-\mathrm{i}(m\phi + n\eta)\} \tag{5}$$

$$\omega'(\theta',\phi',\eta') = \sum_{l=0}^{\infty}\sum_{m=-l}^{l}\sum_{n=-l}^{l} W'^*_{lmn} Z_{lmn}(\cos\theta')\exp\{-\mathrm{i}(m\phi' + n\eta')\} \tag{6}$$

$$q(\beta,\alpha,\gamma) = \sum_{l=0}^{\infty}\sum_{m=-l}^{l}\sum_{n=-l}^{l} V^*_{lmn} Z_{lmn}(\cos\beta)\exp\{-\mathrm{i}(m\alpha + n\gamma)\} \tag{7}$$

where

$$W^*_{lmn} = A_{lmn} + \mathrm{i}B_{lmn}$$

$$W'^*_{lmn} = A'_{lmn} + \mathrm{i}B'_{lmn}$$

$$V^*_{lmn} = Q_{lmn} + \mathrm{i}H_{lmn}$$

The normalized orientation function of the *j*th reciprocal lattice vector $q_j(\theta_j,\phi_j)$ within the specimen can be defined by a series of spherical harmonics as follows:

dx.doi.org/10.1021/jp310239q | J. Phys. Chem. B 2013, 117, 2516−2526

$$q_j(\theta_j,\phi_j) = \sum_{l=0}^{\infty} \sum_{m=-l}^{l} Q_{lm}^{j*} \Pi_l^m(\theta_j) \exp(-im\phi_j) \quad (8)$$

where

$$Q_{lm}^{j*} = A_{lm}^{j} + iB_{lm}^{j}$$

Incidentally, $Z_{lmn}(x)$ in eqs 5−7 is related to Jacobi polynomial, and at $n = 0$ $\Pi_l^m(x) = Z_{lm0}(x)$ in eq 8 is defined as the normalized associated Legendre polynomial.

By using the established general evaluation,[14−17] the geometrical relationships among four functions, $\omega(\theta,\phi,\eta)$, $\omega'(\theta',\phi',\eta')$, $q(\beta,\alpha,\gamma)$, and $q_j(\theta_j,\phi_j)$ are proposed in the Appendix, when crystal units and crystal blocks are oriented symmetrically around the reference axis, X_3 axis, corresponding to external excitation direction of the specimen.

Such a general description can be applied to the industrial composite system where crystal fibers as reinforce material are embedded in amorphous medium and the resultant composite is stretched by drawing machine and/or squeezed by extruder. In this system, the crystallites are oriented with respect to their crystal fiber axis. The orientation function of crystallites by deformation of the composite can be formulated as the general case by using mathematical treatment in the Appendix.

3.3. Application to Orientation of CF Axes with Respect to Magnetic Field Direction. The general description in the Appendix can be applied to the orientation of CF axes with respect to the magnetic field direction as the simplest case. To facilitate understanding the orientation relation between CF axes and the *c*-axes with respect to magnetic field direction, Figure 4 is proposed, in which (a) is a schematic diagram of the *c*-axis and the [002] direction with respect to the CF axis, (b) shows the *c*-axis within a Cartesian coordinate of the CF, and (c) shows the orientation of the CF axis within a Cartesian coordinate of O-$X_1X_2X_3$ of composite (X_3: magnetic field direction). As for a CF, the *c*-axes perpendicular to the [002] axis are oriented randomly around a CF axis and are also rotated randomly around its own axis as shown in Figure 4c. Hence eq A-22 reduces to

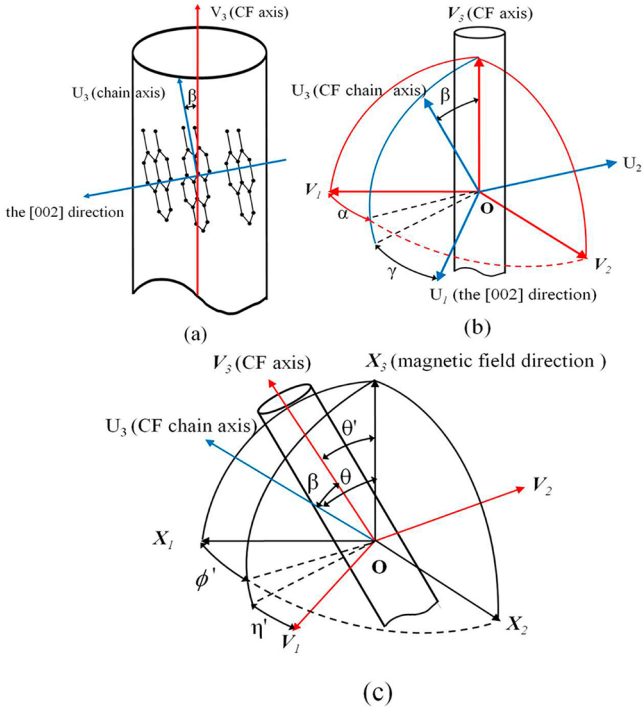

Figure 4. (a) Schematic diagram of the graphite crystal unit representing a Cartesian coordinate of O-$U_1U_2U_3$. (b) Schematic diagram of graphite crystal unit representing a Cartesian coordinate of O-$U_1U_2U_3$ with respect to a Cartesian coordinate O-$V_1V_2V_3$ of bulk carbon fiber. (c) Schematic diagram of bulk carbon fiber representing O-$V_1V_2V_3$ with respect to a Cartesian coordinate O-$X_1X_2X_3$ of space, in which X_3 is the magnetic field direction.

$$Q_{l00} = \int_{\gamma=0}^{2\pi}\int_{\alpha=0}^{2\pi}\int_{\beta=0}^{\pi} q(\beta)\, P_{l00}(\cos\beta)\sin\beta\, d\beta\, d\alpha\, d\gamma = 4\pi^2 \int_0^{\pi} q(\beta)\, P_{l00}(\beta)\sin\beta\, d\beta \quad (9)$$

As discussed before, $q(\beta)$ in eq 9 can be calculated by using eqs 1 ~ 4.

As for CFs, the reciprocal lattice vector of the (002) plane takes uniaxial orientation around the magnetic field direction, in which the rotational angle η defines a random rotation around the X_3 axis in Figure 3a. Furthermore, the reciprocal lattice vector of the (002) plane takes a random orientation around its own CF axis, in which the rotational angle γ specifies a random rotation around the V_3 axis in Figure 3c because of hexagonal crystal unit of graphite and Θ_j' takes 90° shown in Figure 8c in Appendix. Accordingly, eq A-32 reduces to eq 3.

The orientation function $\omega(\theta)$ of the *c*-axes with respect to the magnetic field can be obtained by the function $2\pi q_j(\theta_{[002]})$of the reciprocal lattice vector of the (002) plane with respect to the magnetic field direction experimentally by

$$2\pi q_j(\theta_{[002]}) = \frac{I_{[002]}(\theta_{[002]})}{\int_0^{\pi} I_{[002]}(\theta_{[002]})\sin\theta_{[002]}\, d\theta_{[002]}} \quad (10)$$

where $I_{[002]}(\theta_{[002]})$ is the X-ray diffraction intensity distribution as a function of $\theta_{[002]}$. The experimental method was described as follows:

$$F_{l0}^{[002]} = \int_0^{\pi} q_j(\theta_{[002]})\, P_l(\cos\theta_{[002]})\sin\theta_{[002]}\, d\theta_{[002]} \quad (11)$$

As for CFs under the magnetic field, the reciprocal lattice vector of the (002) plane takes a random orientation around the magnetic field direction, in which the rotational angle η specifies a random orientation around the U_3 axis as shown in Figure 3a and Θ_j takes 90° in Figure 9b in Appendix. Hence

$$F_{l00} = \frac{F_{l0}^{[002]}}{P_l(1)} \quad (12)$$

Considering random orientation for η, eq A-30 reduces to

$$4\pi^2\omega(\theta) = \frac{1}{2} + 2\sum_{l=2}^{\infty} F_{l00}P_l(\cos\theta) \quad (13)$$

Figure 5 shows two kinds of orientation distribution function $2\pi q_j(\theta_{[002]})$ of the [002] direction shown in panels a and $\omega(\theta)$ of chain axes of graphene crystallites in panel b with respect to the magnetic field direction. These functions in the two panels were shown in the previous paper (Figure 6 in ref 1), but they were plotted again in the present paper to set forth the orientation of the CF axes with respect to the magnetic field smoothly. It is seen that the orientation of CFs in 1% CF dispersed solution is less pronounced with increasing PVA concentration. As discussed in the previous paper,[1] this is obviously due to a drastic increase in viscosity of the dispersed solution. The orientation of the chain

dx.doi.org/10.1021/jp310239q | J. Phys. Chem. B 2013, 117, 2516−2526

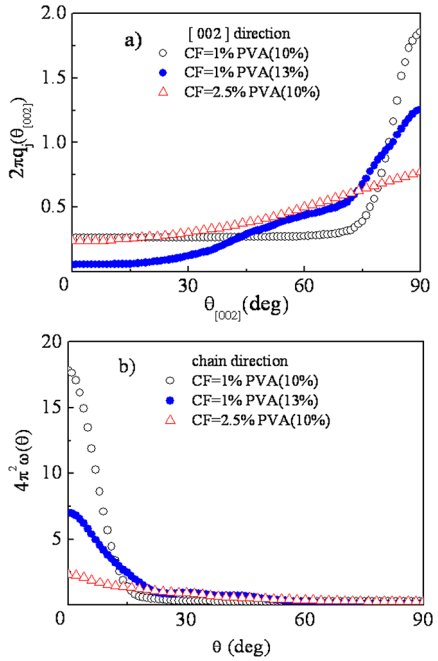

Figure 5. (a) Orientation distribution functions of $2\pi q(\theta_{[002]})$ of the reciprocal lattice vector of the (002) plane ([002]) under the magnetic field. (b) Orientation distribution functions of $4\pi^2\omega(\theta)$ for the carbon chain axis (U_3 axis) calculated by eqs 10−13. These results were shown already in the previous paper (ref 1), and they are shown to facile understanding the present paper.

axes is less pronounced drastically, when CF content increased from 1% to 2.5% in 10% PVA solution, indicating that the collision between adjacent CFs becomes considerable with increasing CF content.

Based on the results in Figures 2 and 5, the orientation function of CF axes with respect to the magnetic field direction can be derived. That is, the coefficient Q_{l00} can be calculated by substituting eq 3 into eq 9, and the orientation factors F'_{l00} of the CF axes with respect to the magnetic field by considering eq 12 can be estimated as follows (see eq A-23)

$$F_{l00} = \int_0^{\pi} \omega'(\theta) Q_{l00} P_l(\cos\theta') \sin\theta' \, d\theta' = Q_{l00} \int_0^{\pi} \omega'(\theta) \, P_l(\cos\theta') \sin\theta' \, d\theta' = F'_{l00} Q_{l00} \tag{14}$$

and

$$F'_{l00} = \frac{F_{l00}}{Q_{l00}} \tag{15}$$

Because of a random orientation of η' in Figure 3b, eq A-31 reduces to eq 16, which denotes the orientation function $\omega'(\theta')$ of CF axes with respect to the magnetic field.

$$4\pi^2\omega'(\theta') = \frac{1}{2} + 2\sum_{l=2}^{\infty} F'_{l00} P_l(\cos\theta') \tag{16}$$

Figure 6 shows the orientation function $\omega'(\theta')$ of the CF axes with respect to the magnetic field direction. The functions suggest that the actual orientation of the CF axes is much steeper than the orientation function of the *c*-axes shown in Figure 5b. This is due to the orientation fluctuation of the *c*-axes with

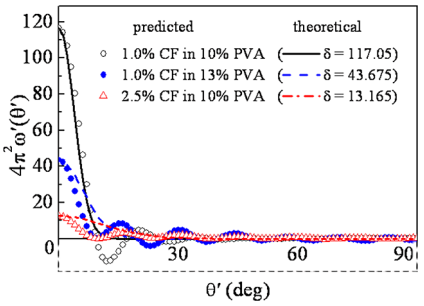

Figure 6. Orientation distribution function of $4\pi^2\omega'(\theta')$ predicted by eqs 14−16 for the CF axes under magnetic field, in which the three kinds of specimen were prepared by the method listed in the panel. The corresponding solid, dashed, and dotted curves were calculated as a function of δ by eqs 19−20.

respect to the CF axis and the reason is obviously conceived to be reasonable through a series of calculations. The waves of the function are attributed to the vibration of the Legendre polynomial $P_l(\cos\theta')$ appeared at higher order of l. The wave magnitude becomes remarkable as the profile of $\omega'(\theta')$ becomes sharper. This means that the functions with very sharp orientation mode have the limit expansion by a series of spherical harmonics as like eqs 5−8. However, there is no way, because the series expansion of Legendre function up to high order beyond $l = 20$ is needed for sharp function but the adopted Legendre polynomial at the high order provides its intrinsic vibration.[17−19] Anyhow, the steep orientation functions of the CF axes with respect to the magnetic field direction are in good agreement with the CF functions observed by SEM images. A series of mathematical evaluation is an indispensable method to resolve apparent contradiction between X-ray diffraction images and SEM observation.

3.4. Orientation Function of CFs at Equilibrium State Estimated by the Energy Concerning Volume Anisotropic Diamagnetic Susceptibility and Magnetic Field. As discussed in the previous paper,[1] the predicted orientation function can be analyzed in comparison with the magnetic orientation of CF axes in solution or gel at the equilibrium state calculated by the magnetic energy of CF. Under a magnetic field, the theoretical orientation of a single CF with susceptibility anisotropy at the equilibrium state may be given by

$$\omega'(\theta') = \frac{\exp\left(-\frac{U}{kT}\right)}{\int_0^{2\pi}\int_0^{2\pi}\int_0^{\pi} \exp\left(-\frac{U}{kT}\right) \sin\theta' \, d\theta' \, d\phi' \, d\eta'} = \frac{\exp\left(-\frac{U}{kT}\right)}{4\pi^2 \int_0^{\pi} \exp\left(-\frac{U}{kT}\right) \sin\theta' \, d\theta'} \tag{17}$$

where k and T are the Bolzmann constant and the absolute temperature, respectively, and U is the magnetic energy under the applied magnetic flux density B, which is given by

$$U = -\frac{\chi_a B^2 V \cos^2\theta'}{2\mu_o} - \frac{\chi_\perp B^2 V}{2\mu_o} \tag{18}$$

where μ_o and V are the magnetic permeability of vacuum and the volume of the particle under consideration, and χ_a is associated with anisotropic diamagnetic susceptibility related to $|\chi_\parallel - \chi_\perp|$, in which $\chi_\parallel$ and $\chi_\perp$ are the anisotropic susceptibilities parallel and perpendicular to the CF axis, respectively. θ' is the angle between

dx.doi.org/10.1021/jp310239q | J. Phys. Chem. B 2013, 117, 2516−2526

CF axis and the applied magnetic field directions (Figures 3b and 4c).

Substituting eq 18 into eq 17 to calculate the orientation function $\omega'(\theta')$ of the CF axes, the second term on the right-hand side in eq 18 is independent of the profile of $\omega'(\theta')$. Then, eq 17 may be rewritten as

$$4\pi^2\omega'(\theta') = \frac{\exp(\delta \cos^2\theta')}{\int_0^\pi \exp(\delta \cos^2\theta') \sin\theta' \, d\theta'} \tag{19}$$

where

$$\delta = \frac{\chi_a V B^2}{2\mu_o kT} = cB^2 \tag{20}$$

The solid, dashed, and dotted curves calculated by eqs 19 and 20 are added in Figure 6. The function $\omega'(\theta')$ provides a sharper profile with an increase in δ value. Incidentally, δ is used as a parameter, instead of γ used in the previous paper,[1] because γ was adopted as a symbol already to represent the orientation in Figure 1c. The theoretical functions show a monotonous decreasing curve with a maximum at $\theta' = 0°$. The theoretical curves are in slightly good agreement with the curves predicated for 1% CFs in 10% and 13% PVA solution and 2.5% CFs in 10% PVA solution by selecting the value of δ. The δ value used for curve fitting of orientation of CF axes in Figure 6 is much higher than that used for curve fitting of the c-axes in the previous paper.[1]

Generally, it may be noted that a macroscopic orientation can occur when the first term in eq 18 exceeds the thermal energy kT represented as $V > 2kT\mu_o/\chi_a B^2$. This indicates that there exist the estimation of minimum critical volume V needed for the orientation given as a function of the applied magnetic flux density B and the anisotropic diamagnetic susceptibility χ_a. As a well-known fact,[20,21] the origin of the magnetic anisotropy is traced back to chemical bonds. The magnetic anisotropy due to chemical bonds provides that diamagnetic susceptibilities for CF. That is, when the magnetic field is applied perpendicular to carbon net-like planar structure with hexagonal shape, the electric current flows along the ring structure to cancel out the magnetic field in accordance with Lenz's law. Hence, stacking direction of the layered structure is oriented perpendicular to the magnetic field by torque, and consequently, the CF axis perpendicular to the stacking direction are oriented parallel to the magnetic field direction.

The orientation of the particles like CFs under magnetic field needs their volume to ensure thermal energy higher than the thermal disturbance. This indicates that at a constant of B, real χ_a given by $|\chi_{\parallel} - \chi_{\perp}|$ for the CF must be higher than the value estimated by orientation of CF chain axes.

As described before, the orientation fluctuation of CF chain axes with respect to the CF axis must be taken into consideration. Actually, even in the high alignment system of CFs with respect to the magnetic field, the X-ray pattern shows broad diffraction arcs different from the sharp spots as has been observed for ultradrawn polyethylene and polypropylene fibers.[11,22]

The value of $\delta = 117.05$ at 1% CFs in 10% PVA solution is much higher than the value 16.8 obtained by curve fitting for the orientation of the c-axes.[1] At $\delta = 117.05$, the anisotropic diamagnetic susceptibility χ_a is calculated to be 5.27×10^{-9}, which is higher than 7.57×10^{-10} calculated at δ (i.e., γ) = 16.8.[1] Even so, the value of 5.27×10^{-9} is much lower than the established values (10^{-5}–10^{-4}) for several kinds of intrinsic CF.[4,5,9,20,21] Judging from the profile of $\omega'(\theta')$ at $\delta = 117.05$, indicating almost perfect orientation of CF axes with respect to the magnetic field direction, such contradiction is probably thought to be due to the fact that the anisotropic diamagnetic susceptibility χ_a is dependent upon the graphitization degree. As reported for the present CFs elsewhere,[10] the graphitization degree is postulated to be lower than the CFs as has been used for measuring intrinsic χ_a because of broad half-width of the (002) plane and indistinct overlapped peaks for the (101), (004), (100), and (112) planes appeared at higher side of twice the Bragg angle in the horizontal direction.[10]

3.5. Time Dependence of the Orientation Function of CFs Using Diffusion Theory. To pursue further detailed estimation for the magnetic orientation of CFs, it may be expected that the orientation of CF axes are attributed to the rotation of the CF axes in the magnetic field direction. In this case, the distribution function $\omega'(\theta',t)$ of CFs with respect to the magnetic field direction may satisfy the following diffusion equation.[23,24]

$$\frac{\partial\omega'(\theta',t)}{\partial t} = \kappa\nabla^2\omega'(\theta',t) - \mathrm{div}\left(\omega'(\theta',t)\frac{\tau}{\varsigma}\right) \tag{21}$$

where κ is the rotational diffusion coefficient of CF axes in the solution. τ is torque, ς is the rotational fractional coefficient, and the symbol ∇^2 is the Laplacian operator. κ is given by $(kT)/\varsigma$. Because a short CF is surely a rigid cylinder such as tobacoo-mosaic virus, κ is given by[1,25]

$$\kappa = \frac{3kT}{8\pi\eta_o a^3}\left\{ln2p - 1.57 + 7\left(\frac{1}{ln2p} - 0.28\right)^2 \pm 0.2^5\right\} = \frac{kT}{\varsigma} \tag{22}$$

where a is an average half-length of CFs and p is an average aspect ratio. η_o is the viscosity of the CF dispersed PVA solution. τ is given by

$$\tau = -\frac{\chi_a V}{\mu_o}B^2 \sin\theta' \cos\theta' \tag{23}$$

As solution of eq 21 by using perturbation method, the distribution function $\omega'(\theta',t)$ is given by

$$\omega'(\theta',t) = \sum_{n=0}^{\infty} W_n y_n \exp\left(\frac{\delta \cos^2\theta'}{2}\right)\exp(-\lambda_n\kappa t) \tag{24}$$

where W_n, λ_n, and y_n are the expansion coefficients described in the previous paper.[1]

Figure 7 shows the orientation functions calculated at the indicated value of κt for 2.5% CFs in solution with 10% PVA solution. The other cases could not be calculated numerically because the orientation function $\omega'(\theta',t)$ is too sharp to adopt perturbation method for obtaining solution of eq 21. The theoretical calculation for the indicated dispersed solutions was done by using the same value of δ, 13.165, associated with each equilibrium state for 2.5% CFs in solution with 10% PVA solution in Figure 5. The termination up to $l = 18$ was the best to give the stable profile by the suppression of wave magnitude of the function as small as possible. The theoretical curve profile with a maximum peak at $\theta' = 0°$ becomes sharper with increasing κt, and the value at $\theta' = 0°$ closes to the corresponding saturated curves with many waves in Figure 6.

dx.doi.org/10.1021/jp310239q | J. Phys. Chem. B 2013, 117, 2516–2526

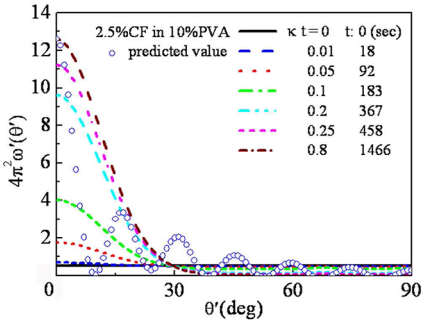

Figure 7. Orientation distribution function of $4\pi^2\omega'(\theta')$ (open circles) predicted by eqs 14−16 at the equilibrium state, which is measured for 2.5% CF in 10% PVA solution. The curves are calculated as a function of κt by eq 24.

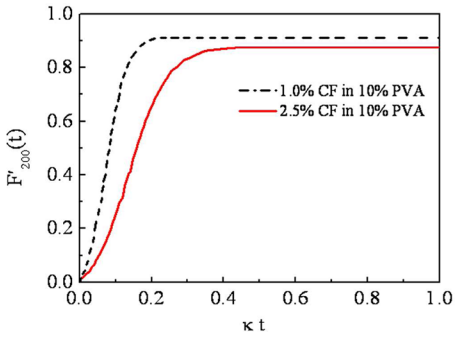

Figure 8. Second-order orientation factor $F'_{200}(t)$ of CF axes calculated by eq 25 for dispersed 10% PVA solutions with 1% and 2.5% CF contents.

Figure 8 shows the second-order orientation factor given by

$$F'_{200}(t) = \int_0^{\pi} \omega'(\theta')\, P_2(\cos\theta')\, \sin\theta'\, d\theta' \tag{25}$$

The value of $F'_{200}(t)$ becomes unity for perfect orientation of the CF axes with respect to the magnetic field direction (film normal direction), but it becomes zero for a random orientation. The factor increases drastically with increasing κt and tends to level off. The value of $F'_{200}(t)$ is only the second-order moment of $\omega'(\theta',t)$ but the increasing outline of the orientation degree of CF axes with elapsing time can be figured out simply. From Figure 8, it is easy to understand such behavior that an increase in PVA concentration causes a drastic increase in viscosity and the orientation of CF axes becomes less significant and an increase in CF content is related to drastic collision between adjacent CFs under magnetic orientation.

Different from predominant orientation of CFs and carbon nanotubes (CNTs)−polymer composite by ultradrawing,[26,27] the magnetic field is needed to realize the preferential orientation of CF axes parallel to the film thickness direction. Certainly, CNTs and ultrahigh molecular weight polyethylene (UHMWPE) composites could be elongated more than 100 times, when the composites were prepared by gelation/crytasallization and the drawn composites provided high electron conductivity and high modulus. However, the ultradrawn method is not effective on obtaining the composites where the CFs and CNTs are oriented predominantly with respect to the film thickness direction. Accordingly, the orientation of CFs and CNTs have currently drawn much attention for many industrial materials and a number of papers have reported for the magnetic effect of diamagnetism in relation to the induced motion of electrons under the magnetic field.[28−36]

4. CONCLUSIONS

The evaluation method for the orientation of the CF axes with respect to the magnetic field was proposed in the case that the *c*-axes (crystal chain axes) have orientation distribution with respect to the CF axis. The mathematical description was achieved in such a general case that crystal blocks (such as fiber), whose crystal chain axes have random rotation around their own axis, were imbedded in the amorphous medium and the composite was deformed. The orientation function of the blocks was formulated with respect to the external excitation direction. As the simplest case, the orientation of CF axes with respect to the magnetic field direction was calculated and the predicted results were discussed in comparison to the orientation of CF chain axes. The predicted functions of CF axes were sharper than the corresponding function of the *c*-axes. This was attributed to the orientation distribution of the *c*-axes with respect to the CF axis. Actually in spite of almost perfect orientation of CF fibers observed under SEM, the corresponding WAXD image from the (002) plane showed broad diffraction arcs different from strong intensity spots observed ultradrawn polyethylene and polypropylene. Such contradiction for CFs could be resolved by considering the orientation distribution of the *c*-axes with respect to their CF axis.

APPENDIX

Let us consider a given *j*th reciprocal lattice vector $\mathbf{r}_j$ fixed within the crystal unit. The orientation of the vector $\mathbf{r}_j$ may also be specified by three sets of polar and azimuthal angles, (θ_j, ϕ_j), (Θ_j, Φ_j), and (Θ'_j, Φ'_j) with respect to these coordinates, O-$X_1X_2X_3$, O-$U_1U_2U_3$, and O-$V_1V_2V_3$, respectively. Figure 9a illustrates the orientation of $\mathbf{r}_j$ vector with the O-$X_1X_2X_3$ coordinate, the reference coordinate being along the X_3 axis, and Figures 9b,c correspond to the orientation of $\mathbf{r}_j$ with O-$U_1U_2U_3$ and $V_1V_2V_3$ coordinates, respectively. The relationships among the indicated angles are given by

$$\begin{pmatrix} \sin\theta_j \cos\phi_j \\ \sin\theta_j \sin\phi_j \\ \cos\theta_j \end{pmatrix} = T(\theta,\phi,\eta) \begin{pmatrix} \sin\Theta_j \cos\Phi_j \\ \sin\Theta_j \sin\Phi_j \\ \cos\Theta_j \end{pmatrix} \tag{A-1}$$

$$\begin{pmatrix} \sin\theta_j \cos\phi_j \\ \sin\theta_j \sin\phi_j \\ \cos\theta_j \end{pmatrix} = T(\theta',\phi',\eta) \begin{pmatrix} \sin\Theta'_j \cos\Phi'_j \\ \sin\Theta'_j \sin\Phi'_j \\ \cos\Theta'_j \end{pmatrix} \tag{A-2}$$

$$\begin{pmatrix} \sin\Theta'_j \cos\Phi'_j \\ \sin\Theta'_j \sin\Phi'_j \\ \cos\Theta'_j \end{pmatrix} = T(\beta,\alpha,\gamma) \begin{pmatrix} \sin\Theta_j \cos\Phi_j \\ \sin\Theta_j \sin\Phi_j \\ \cos\Theta_j \end{pmatrix} \tag{A-3}$$

where, for example,

dx.doi.org/10.1021/jp310239q | J. Phys. Chem. B 2013, 117, 2516−2526

$$T(\beta, \alpha, \gamma) = \begin{pmatrix} \cos\alpha\cos\beta\cos\gamma - \sin\alpha\sin\gamma & -\cos\alpha\cos\beta\sin\gamma - \sin\alpha\cos\gamma & \cos\alpha\sin\beta \\ \sin\alpha\cos\beta\cos\gamma + \cos\alpha\sin\gamma & -\sin\alpha\cos\beta\sin\gamma + \cos\alpha\cos\gamma & \sin\alpha\sin\beta \\ -\sin\beta\sin\gamma & \sin\beta\sin\gamma & \cos\beta \end{pmatrix} \quad \text{(A-4)}$$

With eqs A-1−A-3, a generalization of the Legendre addition theorem gives the following relations

$$\Pi_l^m(\cos\theta_j)\exp(im\phi_j) = \left(\frac{2}{2l+1}\right)^{1/2}\sum_{n=-l}^{l} Z_{lmn}(\cos\theta)\exp\{i(m\phi + n\eta)\} \times \Pi_l^n(\cos\Theta_j)\exp(in\Phi_j) \quad \text{(A-5)}$$

$$\Pi_l^m(\cos\theta_j)\exp(im\phi_j) = \left(\frac{2}{2l+1}\right)^{1/2}\sum_{n=-l}^{l} Z_{lmn}(\cos\theta')\exp\{i(m\phi' + n\eta')\} \times \Pi_l^n(\cos\Theta'_j)\exp(in\Phi'_j) \quad \text{(A-6)}$$

$$\Pi_l^m(\cos\Theta'_j)\exp(im\Phi'_j) = \left(\frac{2}{2l+1}\right)^{1/2}\sum_{s=-l}^{l} Z_{lsn}(\cos\beta)\exp\{i(s\alpha + n\gamma)\} \times \Pi_l^n(\cos\Theta_j)\exp(in\Phi_j) \quad \text{(A-7)}$$

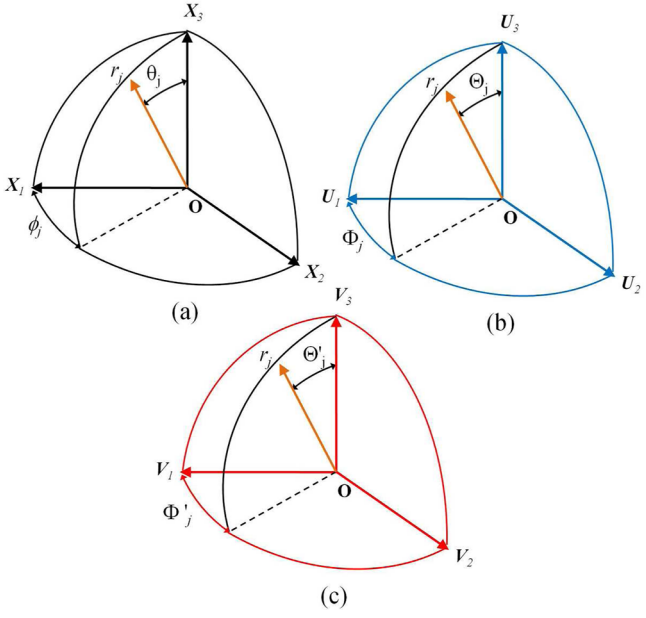

Figure 9. Cartesian coordinates illustrating the geometrical relations. (a) Angles θ_j and ϕ_j, which specify the orientation of the given jth axis of the crystal unit with respect to the coordinate O-$X_1X_2X_3$ of bulk specimen. (b) Angles Θ_j and Φ_j, which specify the orientation of the given jth axis of the crystal unit with respect to the coordinate O-$U_1U_2U_3$ of crystal unit cell. (c) Angles Θ'_j and Φ'_j, which specify the orientation of the given jth axis of the crystal unit with respect to the coordinate O-$V_1V_2V_3$ of crystal block.

Multiplying both sides of eq A-5 by $\omega(\theta,\phi,\eta)\cdot q(\theta_j,\phi_j)$ and integrating over all angles in the space, θ, ϕ, η, θ_j, ϕ_j, one can obtain the following relation

$$Q_{lm}^{j*} = 2\pi\left(\frac{2}{2l+1}\right)^{1/2}\sum_{n=-l}^{\infty} W_{lmn}^{*}\Pi_l^n(\cos\Theta_j)\exp(in\Phi_j) \quad \text{(A-8)}$$

Similarly, multiplying both sides of eq A-6 by $\omega'(\theta,\phi,\eta)\cdot q(\theta_j,\phi_j)$ and integrating over all angles in the space, θ', ϕ', η', θ_j, ϕ_j, one can obtain the following relation

$$Q_{lm}^{j*} = 2\pi\left(\frac{2}{2l+1}\right)^{1/2}\sum_{n=-l}^{\infty} W_{lms}'^{*}\Pi_l^s(\cos\Theta'_j)\exp(is\Phi'_j) \quad \text{(A-9)}$$

For general industrial products, there may exist the following orthogonally biaxial symmetry of the orientation distribution function: $q_j(\pm\cos\theta_j,\pm\phi_j) = q_j(\pm\cos\theta_j,\pi\pm\phi_j)$

Hence,

$$Q_{lm}^{j*} = A_{lm}^{j}(B_{lm}^{j}=0) = A_{l\bar{m}}^{j} \qquad (m\text{: even})$$

$$A_{lm}^{j} = 0 \qquad (m\text{: odd})$$

Accordingly, eqs A-8 and A-9 can be simplified as

$$A_{lm}^{j} = 2\pi\left(\frac{2}{2l+1}\right)^{1/2}\{A_{lm0}\Pi_l(\cos\Theta_j) + 2\sum_{n=1}^{l}(A_{lmn}\cos n\Phi_j - B_{lmn}\sin n\Phi_j)\Pi_l^n(\cos\Theta_j)\} \quad \text{(A-10)}$$

and

$$A_{lm}^{j} = 2\pi\left\{\frac{2}{2l+1}\right\}^{1/2}\{A'_{lm0}\Pi_l(\cos\Theta'_j) + 2\sum_{n=1}^{l}(A'_{lmn}\cos n\Phi'_j - B'_{lmn}\sin n\Phi'_j)\Pi_l^n(\cos\Theta'_j)\} \quad \text{(A-11)}$$

In the simple case like an orthogonal (orthorhombic) unit like polyethylene, eqs A-10 and A-11 are rewritten for even numbers of l, m, and n as follows:

$$A_{lm}^{j} = 2\pi\left(\frac{2}{2l+1}\right)^{1/2}\{A_{lm0}\Pi_l(\cos\Theta_j) + 2\sum_{n=2}^{l}A_{lmn}\Pi_l^n(\cos\Theta_j)\cos n\Phi_j\} \quad \text{(A-12)}$$

and

dx.doi.org/10.1021/jp310239q | J. Phys. Chem. B 2013, 117, 2516−2526

$$A_{lm}^{j} = 2\pi\left(\frac{2}{2l+1}\right)^{1/2}\{A'_{lm0}\Pi_l(\cos\Theta'_j) + 2\sum_{n=2}^{l} A'_{lmn}\Pi_l^n(\cos\Theta'_j)\cos n\Phi'_j\} \quad \text{(A-13)}$$

Now, substituting eq A-7 into eq A-6 and comparing the result with eq A-5, one may obtain the following relation

$$Z_{lmn}(\cos\theta)\exp\{\mathrm{i}(m\phi+n\eta)\} = \left(\frac{2}{2l+1}\right)^{1/2}\sum_{s=-l}^{l} Z_{lms}(\cos\theta')\exp\{\mathrm{i}(m\phi'+n\eta')\} \times Z_{lsn}(\cos\beta)\exp\{\mathrm{i}(s\alpha+n\gamma)\} \quad \text{(A-14)}$$

Again, substituting

$$V_{lsn}^{*} = Z_{lsn}(\cos\beta)\exp\{\mathrm{i}(s\alpha+n\gamma)\} = Q_{lsn} + \mathrm{i}H_{lsn} \quad \text{(A-15)}$$

Multiplying both sides of eq A-14 by $\omega(\theta,\phi,\eta)\cdot\omega'(\theta',\phi',\eta')$, and integrating all angles, one obtains the following coefficient by considering the symmetries of specimen and crystal unit. That is,

$$A_{lmn} = \left\{4\pi^2\left(\frac{2}{2l+1}\right)^{1/2}\right\}\sum_{s=-l}^{l}\int_{\eta'=0}^{2\pi}\int_{\phi'=0}^{2\pi}\int_{\theta'=0}^{\pi}\omega'(\theta',\phi',\eta') \times Z_{lms}(\cos\theta')Q_{lsn}\cos(m\phi'+n\gamma')\sin\theta'\,\mathrm{d}\theta'\,\mathrm{d}\phi'\,\mathrm{d}\eta' = \left\{4\pi^2\left(\frac{2}{2l+1}\right)^{1/2}\right\}\sum_{s=-l}^{l} A'_{lmn}Q_{lsn} \quad \text{(A-16)}$$

Similarly, multiplying both sides of eq A-15 by $\omega(\theta,\phi,\eta)\cdot\omega'(\theta',\phi',\eta')\cdot q(\beta,\alpha,\gamma,)$, and integrating all angles, one obtains the following coefficient for the real part. That is,

$$Q_{lsn} = \int_{\gamma=0}^{2\pi}\int_{\alpha=0}^{2\pi}\int_{\beta=0}^{\pi} q(\beta,\alpha,\gamma)Z_{lsn}(\cos\beta) \times \cos(s\alpha+n\gamma)\sin\beta\,\mathrm{d}\alpha\,\mathrm{d}\gamma \quad \text{(A-17)}$$

On the other hand, the coefficients A_{lmn} and A_{lm}^{j} may be considered as a sort of averaged degree of the orientation distribution functions, and generalized orientation factors F_{lmn} and F_{lm}^{j} can be defined as follows

$$F_{lmn} = 4\pi^2\left\{\frac{2}{2l+1}\frac{(l+m)!}{(l-m)!}\frac{(l+n)!}{(l-n)!}\right\}^{1/2}A_{lmn} \quad \text{(A-18)}$$

$$F_{lm}^{j} = 2\pi\left\{\frac{2}{2l+1}\frac{(l+m)!}{(l-m)!}\right\}A_{lm}^{j} \quad \text{(A-19)}$$

$$G_{lsn} = 4\pi^2\left\{\frac{2}{2l+1}\frac{(l+s)!}{(l-s)!}\frac{(l+n)!}{(l-n)!}\right\}^{1/2}Q_{lsn} \quad \text{(A-20)}$$

Similarly, $P_{lmn}(x)$ may be defined as follows

$$P_{lmn}(x) = \left\{\frac{2}{2l+1}\frac{(l+m)!}{(l-m)!}\frac{(l+n)!}{(l-n)!}\right\}Z_{lmn}(x) \quad \text{(A-21)}$$

Thus eqs A-16 and A-17 may be rewritten by using eqs A-19−A-21.

$$Q_{lsn} = \int_{\gamma=0}^{2\pi}\int_{\alpha=0}^{2\pi}\int_{\beta=0}^{\pi} q(\beta,\alpha,\gamma)P_{lsn}(\cos\beta) \times \cos(s\alpha+n\gamma)\sin\beta\,\mathrm{d}\beta\,\mathrm{d}\alpha\,\mathrm{d}\gamma \quad \text{(A-22)}$$

$$F_{lmn} = F'_{lmn}Q_{l0n} + 2F'_{lmn}\sum_{s=2}^{l}\frac{(l-s)!}{(l+s)!}Q_{lsn} \quad \text{(A-23)}$$

$$F'_{lmn} = \frac{F_{lmn}}{Q_{l0n} + 2\sum_{s=2}^{l}\frac{(l-n)!}{(l+n)!}Q_{lsn}} \quad \text{(A-24)}$$

Furthermore, eqs 5−7 are rewritten for the orthorhombic crystal unit like polyethylene as follows

$$4\pi^2\omega(\theta,\phi,\eta) = \frac{1}{2} + 2\sum_{l=2}^{\infty}\frac{2l+1}{2}F_{l00}P_l(\cos\theta) + 2\sum_{l=2}^{\infty}\frac{2l+1}{2}\sum_{m=2}^{l}\frac{(l-m)!}{(l+m)!}F_{lm0}P_l^m(\cos\theta)\cos m\phi + 2\sum_{l=2}^{\infty}\frac{2l+1}{2}\sum_{m=2}^{l}\frac{(l-m)!}{(l+m)!} \times \sum_{n=2}^{l}\frac{(l-n)!}{(l+n)!}F_{lmn}P_{lmn}(\cos\theta)\cos(m\phi+n\eta) \quad \text{(A-25)}$$

$$4\pi^2\omega'(\theta',\phi',\eta') = \frac{1}{2} + 2\sum_{l=2}^{\infty}\frac{2l+1}{2}F'_{l00}P_l(\cos\theta') + 2\sum_{l=2}^{\infty}\frac{2l+1}{2}\sum_{m=2}^{l}\frac{(l-m)!}{(l+m)!}F'_{lm0}P_l^m(\cos\theta')\cos m\phi' + 2\sum_{l=2}^{\infty}\frac{2l+1}{2}\sum_{m=2}^{l}\frac{(l-m)!}{(l+m)!} \times \sum_{n=2}^{l}\frac{(l-n)!}{(l+n)!}F'_{lmn}P_{lmn}(\cos\theta')\cos(m\phi'+n\eta') \quad \text{(A-26)}$$

$$4\pi^2 q(\beta,\alpha,\gamma) = \frac{1}{2} + 2\sum_{l=2}^{\infty}\frac{2l+1}{2}G_{l00}P_l(\cos\beta) + 2\sum_{l=2}^{\infty}\frac{2l+1}{2}\sum_{s=2}^{l}\frac{(l-s)!}{(l+s)!}G_{ls0}P_l^s(\cos\beta)\cos s\alpha + 2\sum_{l=2}^{\infty}\frac{2l+1}{2}\sum_{s=2}^{l}\frac{(l-s)!}{(l+s)!} \times \sum_{n=2}^{l}\frac{(l-n)!}{(l+n)!}G_{lsn}P_{lsn}(\cos\beta)\cos(s\alpha+n\gamma) \quad \text{(A-27)}$$

For uniaxial orientation, the orientation distribution functions contain no terms dependent on the angles, ϕ, ϕ', and ϕ_j. Therefore, eqs A-23−A-27 may be rewritten as follows:

$$F_{l0n} = F'_{l0n}Q_{l0n} + 2F'_{l0n}\sum_{s=2}^{l}\frac{(l-s)!}{(l+s)!}Q_{lsn} \quad \text{(A-28)}$$

$$F'_{l0n} = \frac{F_{l0n}}{Q_{l0n} + 2\sum_{s=2}^{l}\frac{(l-n)!}{(l+n)!}Q_{lsn}} \quad \text{(A-29)}$$

dx.doi.org/10.1021/jp310239q | J. Phys. Chem. B 2013, 117, 2516−2526

$$4\pi^2\omega(\theta,\eta) = \frac{1}{2} + 2\sum_{l=2}^{\infty}\frac{2l+1}{2}F_{l00}P_l(\cos\theta) + 2\sum_{l=2}^{\infty}\frac{2l+1}{2}\sum_{n=2}^{l}\frac{(l-n)!}{(l+n)!}F_{l0n}P_l^n(\cos\theta)\cos n\eta \quad \text{(A-30)}$$

$$4\pi^2\omega'(\theta',\eta') = \frac{1}{2} + 2\sum_{l=2}^{\infty}\frac{2l+1}{2}F'_{l00}P_l(\cos\theta') + 2\sum_{l=2}^{\infty}\frac{2l+1}{2}\sum_{n=2}^{l}\frac{(l-n)!}{(l+n)!}F'_{l0n}P_l^n(\cos\theta')\cos n\eta' \quad \text{(A-31)}$$

$$4\pi^2 q(\beta,\gamma) = \frac{1}{2} + 2\sum_{l=2}^{\infty}\frac{2l+1}{2}G_{l00}P_l(\cos\beta) + 2\sum_{l=2}^{\infty}\frac{2l+1}{2}\sum_{n=2}^{l}\frac{(l-n)!}{(l+n)!}G_{l0n}P_l^n(\cos\beta)\cos n\gamma \quad \text{(A-32)}$$

Incidentally, as for the triclinic unit cell with no symmetry of the reciprocal lattice vector in a crystal unit like poly(ethylene terephthalate), eqs A-30−A-32 can be rewritten as follows:

$$4\pi^2\omega(\theta,\eta) = \frac{1}{2} + 2\sum_{l=2}^{\infty}\frac{2l+1}{2}F^1_{l00}P_l(\cos\theta) + 2\sum_{l=2}^{\infty}\frac{2l+1}{2}\sum_{n=1}^{l}\frac{(l-n)!}{(l+n)!}(F^1_{l0n}\cos n\eta + F^2_{l0n}\sin n\eta)P_l^n(\cos\theta) \quad \text{(A-33)}$$

$$4\pi^2\omega'(\theta',\eta') = \frac{1}{2} + 2\sum_{l=2}^{\infty}\frac{2l+1}{2}F^{1'}_{l00}P_l(\cos\theta') + 2\sum_{l=2}^{\infty}\frac{2l+1}{2}\sum_{n=1}^{l}\frac{(l-n)!}{(l+n)!}(F^{1'}_{l0n}\cos n\eta' + F^{2'}_{l0n}\sin n\eta')P_l^n(\cos\theta') \quad \text{(A-34)}$$

$$4\pi^2 q(\beta,\gamma) = \frac{1}{2} + 2\sum_{l=2}^{\infty}\frac{2l+1}{2}G^1_{l00}P_l(\cos\beta) + 2\sum_{l=2}^{\infty}\frac{2l+1}{2}\sum_{n=1}^{l}\frac{(l-n)!}{(l+n)!}(G^1_{l0n}\cos n\gamma + G^2_{l0n}\sin n\gamma)P_l^n(\cos\beta) \quad \text{(A-35)}$$

Anyway, eqs A-33 (and A-30) and A-35 (and eq A-32) can be obtained by X-ray measurements using eqs A-22−A-24 and then the orientation of embedded crystal blocks (like fibers) can be obtained by eq A-34 (and eq A-31) to investigate the characteristics of reinforced composites.

AUTHOR INFORMATION

Corresponding Author

*E-mail: mm-matsuo@live.jp.

Notes

The authors declare no competing financial interest.

ACKNOWLEDGMENTS

The authors are indebted to Prof. Kimura of Kyoto University who has developed magnetic orientation of polymer chains.

REFERENCES

(1) Nakano, Y.; Matsuo, M. Orientation Behavior of Carbon Fiber Axes in Polymer Solutions under Magnetic Field Estimated in Terms of Orientation Distribution Function. *J. Phys. Chem. C* **2008**, *112*, 15611−15622.

(2) Timbrell, V. Alignment of Carbon and Other Man-made Fibers by Magnetic Fields. *J. Appl. Phys.* **1972**, *43*, 4839−4840.

(3) Matthews, M. J.; Dresselhaus, M. S.; Dresselhaus, G.; Endo, M.; Nishimura, Y.; Hiraoka, T.; Tamaki, N. Magnetic Alignment of Mesophase Pitch-based Carbon Fibers. *Appl. Phys. Lett.* **1996**, *69*, 430−432.

(4) Fujiwara, M.; Oki, E.; Hamada, M.; Tanimoto, Y.; Mukouda, I.; Shimomura, Y. Magnetic Orientation and Magnetic Properties of a Single Carbon Nanotube. *J. Phys. Chem. A* **2001**, *105*, 4383−4386.

(5) Kimura, T.; Ago, H.; Tobita, M.; Ohshima, S.; Kyotani, M.; Yumura, M. Polymer Composites of Carbon Nanotubes Aligned by a Megnetic Field. *Adv. Mater.* **2002**, *14*, 1380−1383.

(6) Casavant, M. J.; Walters, D. A.; Schmidt, J. J.; Smalley, R. E. Neat Macroscopic Membranes of Aligned Carbon Nanotubes. *J. Appl. Phys.* **2003**, *93*, 2153−2156.

(7) Fischer, J. E.; Zhou, W.; Vavro, J.; Llaguno, M. C.; Guthy, C.; Haggenmueller, R.; Casavant, M. J.; Walters, D. E.; Smalley, R. E. Magnetically Aligned Single Wall Carbon Nanotube Films: Preferred Orientation and Anisotropic Transport Properties. *J. Appl. Phys.* **2003**, *93*, 2157−2163.

(8) Takahashi, T.; Yonetake, K.; Koyama, K.; Kikuchi, T. Polycarbonate Crystallization by Vapor-Grown Carbon Fiber with and without Magnetic Field. *Macromol. Rapid Commun.* **2003**, *24*, 763−767.

(9) Takahashi, T.; Suzuki, K.; Awano, H.; Yonetake, K. Alignment of Vapor-grown Carbon Fibers in Polymer under Magnetic Field. *Chem. Phys. Lett.* **2007**, *436*, 378−382.

(10) Kaburagi, M.; Bin, Y.; Zhu, D.; Xu, C.; Matsuo, M. Small Angle X-ray Scattering from Voids within Fibers during the Stabilization and Carbonization Stages. *Carbon* **2003**, *41*, 915−926.

(11) Matsuo, M.; Sawatari, C.; Iida, M.; Yoneda, M. Ultradrawing of High Molecular Weight Polyethylene Films Produced by Gelation/Crystallization from Solution: Effect of the Number of Entanglements. *Polym. J. (Tokyo, Jpn.)* **1985**, *17*, 1197−1208.

(12) Roe, R. J.; Krigbaum, W. R. Description of Crystallite Orientation in Polycrystalline Materials Having Fiber Texture. *J. Chem. Phys.* **1964**, *40*, 2608−2615.

(13) Krigbaum, W. R.; Roe, R. J. Crystallite Orientation in Materials Having Fiber Texture. II. A Study of Strained Samples of Crosslinked Polyethylene. *J. Chem. Phys.* **1964**, *41*, 737−748.

(14) Roe, R. J. Description of Crystallite Orientation in Polycrystalline Materials. III.General Solution to Pole Figure Inversion. *J. Appl. Phys.* **1965**, *36*, 2024−2031.

(15) Matsuo, M.; Adachi, R.; Jiang, X.; Bin, Y. Orientation Behavior of the Three Principal Crystallographic Axes of Poly(butylene terephthalate) Estimated in Terms of Orientation Distribution Function of Crystallites. *Macromolecules* **2004**, *37*, 1324−1332.

(16) Bin, Y.; Oishi, K.; Yoshida, K.; Nakashima, T.; Matsuo, M. Orientation Distribution Functions of the Three Principal Crystallographic Axes as well as Crystallites of Poly(ethylene terephthalate) Films under Biaxially Stretching. *Polym. J. (Tokyo, Jpn.)* **2004**, *36*, 394−402.

(17) Matsuo, M.; Sawatari, C.; Iwai, Y.; Ozaki, F. Effect of Orientation Distribution and Crystallinity on the Measurement by X-ray Diffraction of the Crystal Lattice Moduli of Cellulose I and II. *Macromolecules* **1990**, *23*, 3266−3275.

(18) Matsuo, M.; Ooki, J.; Harashina, Y.; Ogita, T.; Manley, R. S. Theoretical Estimation of Segmental Orientation in Deformed Polymeric Networks Using a Lattice Model and Application to Orientation of Amorphous Chain Segments of Poly(ethylene

terephthalate) and Oriented Crystallization of Polyethylene. *Macromolecules* **1995**, *28*, 4951−4960.
(19) Matsuo, M.; Sugiura, Y.; Kimura, T.; Ogita, T. Segmental Orientation in Uniaxially Deformed Polymer Networks and Application to Orientation-Induced Crystallization. *Macromolecules* **2002**, *35*, 4493−4509.
(20) Kimura, Y.; Yoshino, M.; Koshimuzu, W.; Koike, M.; Kawai, T. Magnetic Orientation of Polymer Fibers in Suspension. *Langumuir* **2000**, *16*, 858−861.
(21) Kimura, T. Study on the Effect of Magnetic Fields on Polymeric Materials and Its Application. *Polym. J. (Tokyo, Jpn.)* **2003**, *35*, 823−843.
(22) Sawatari, C.; Matsuo, M. Temperature Dependence of Crystal Lattice Modulus and Dynamic Mechanical Properties of Ultradrawn Polypropylene Films. *Macromolecules* **1989**, *22*, 2968−2973.
(23) Matsumoto, M.; Watanabe, H.; Yoshioka, K. The Transient Electric Birefringence of Rigid Macromolecules in Solution under the Action of a Rectangular Pulse and a Reversing Pulse. *J. Phys. Chem.* **1970**, *74*, 2182−2188.
(24) Matsuo, M.; Kakei, K.; Nagaoka, Y. Light Scattering Studies on the Deformation Mechanism of Liquid Crystals under Electric and Magnetic Field. *J. Chem. Phys.* **1981**, *75*, 5925−5939.
(25) Broersma, S. Rotational Diffusion Constant of a Cylindrical Particle. *J. Chem. Phys.* **1960**, *32*, 1626−1631.
(26) Bin, Y.; Kitanaka, M.; Zhu, D.; Matsuo, M. Development of Highly Oriented Polyethylene Filled with Aligned Carbon Nanotubes by Gelation/Crystallization from Solutions. *Macromolecules* **2003**, *36*, 6213−6219.
(27) Bin, Y.; Chen, Q.; Tashiro, K.; Matsuo, M. Electrical and Mechanical Properties of Iodine-doped Highly Elongated Ultrahigh Molecular Weight Polyethylene Films Filled with Multiwalled Carbon Nanotubes. *Phys. Rev. B* **2008**, *77*, 035419−035425.
(28) Beaugnon, E.; Tournier, R. Levitation of Organic Materials. *Nature (London)* **1991**, *349*, 470.
(29) Berry, M. V.; Geim, A. K. Of Flying Frogs and Levitrons. *Eur. J. Phys.* **1997**, *18*, 307−313.
(30) Kitamura, N.; Makihara, M.; Hamai, M.; Sato, T.; Mogi, I.; Awaji, S.; Watanabe, K.; Motokawa, M. Containerless Melting Glass by Magnetic Levitation Method. *Jpn. J. Appl. Phys. Part 2* **2000**, *39*, L324−L326.
(31) Fujiwara, M.; Chidiwa, T.; Tokunaga, R.; Tanimoto, Y. Crystal Growth of *trans*-Azobenzene in a Magnetic Field of 80 kOe. *J. Phys. Chem B* **1998**, *102*, 3417−3419.
(32) Fujiwara, M.; Fukui, M.; Tanimoto, Y. Magnetic Orientation of Benzophenone Crystals in Fields up to 80.0 KOe. *J. Phys. Chem. B* **1999**, *103*, 2627−2630.
(33) Sugiyama, J.; Chanzy, H.; Maret, G. Orientation of Cellulose Microcrystals by Strong Magnetic Fields. *Macromolecules* **1992**, *25*, 4232−4234.
(34) Revol, J. F.; Godbout, L.; Dong, X. M.; Gray, D. G.; Chanzy, H.; Maret, G. Chiral Nematic Suspensions of Cellulose Crystallites; Phase Separation and Magnetic Field Orientatiion. *Liq. Cryst.* **1994**, *16*, 127−134.
(35) Dong, X. M.; Gray, D. G. Induced Circular Dichroism of Isotropic and Magnetically-Oriented Chiral Nematic Suspensions of Cellulose Crystallites. *Langmuir* **1997**, *11*, 3029−3034.
(36) Kimura, T.; Kawai, T.; Sakamoto, Y. Magnetic orientation of poly(ethylene terephthalate). *Polymer* **2000**, *41*, 809−812.